sustainability

MDPI

Article

Vapor Phase Alkylation of Isomeric Cresols with *Tert*-Butyl Alcohol over Perlite Supported Sulfated Zirconia Catalyst

Sakshi Kabra Malpani [1], Deepti Goyal [2], Sampath Chinnam [3], Sunil K. Sharma [4], Stuti Katara [5] and Ashu Rani [5,*]

[1] Department of Chemistry and Biochemistry, Jyoti Nivas College Autonomous, Bengaluru 560095, Karnataka, India; sakshikmalpani@gmail.com
[2] Department of Applied Chemistry, School of Vocational Studies & Applied Sciences, Gautam Buddha University, Greater Noida 201308, Uttar Pradesh, India; deepti_skjain@yahoo.com
[3] Department of Chemistry, M.S. Ramaiah Institute of Technology, Visvesvaraya Technological University, Bengaluru 560054, Karnataka, India; sampathchinnam@gmail.com
[4] Department of Chemistry, State University of New York, New York, NY 11790, USA; sk5040@gmail.com
[5] Department of Pure and Applied Chemistry, University of Kota, Kota 324005, Rajasthan, India; stuti27oct@gmail.com
* Correspondence: ashu.uok@gmail.com

Abstract: In the present study, perlite was thermally activated and then modified desirably to generate super acidity by loading different weight percentages of sulfated zirconia (SZ) via the two-step sol-gel method. As-prepared sulfated zirconia perlite (SZP) catalysts showed suitable catalytic potential in the vapor phase alkylation of *o*, *m*, and *p*-cresols with *tert*-butyl alcohol. The presence of crystalline phases in SZP catalysts was confirmed by XRD and FT-IR studies. TEM images revealed the nano size of the catalysts in the range of 9–25 nm. The presence of SZ on the surface of perlite was further confirmed by N_2 adsorption–desorption, SEM, SEM-EDX, TGA, and UV-Vis DRS techniques. The pyridine FT-IR results confirmed the existence of Brønsted, Lewis acidic sites and their combination as super acidic catalytic active centers on the surface of catalyst utilized in the vapor phase alkylation of *o*, *m*, and *p*-cresols with *tert*-butyl alcohol. The regeneration and reusability of the preferred catalyst until the 5th reaction cycle without any considerable loss in catalytic activity demonstrated the stability of the catalyst. Comparative studies show that SZP can be regenerated and is superior compared to other catalysts previously used for other alkylation reactions with the potential for use on a large scale.

Keywords: perlite; sulfated zirconia; vapor phase; alkylation; cresols; *tert*-butyl alcohol; reusability

Citation: Malpani, S.K.; Goyal, D.; Chinnam, S.; Sharma, S.K.; Katara, S.; Rani, A. Vapor Phase Alkylation of Isomeric Cresols with *Tert*-Butyl Alcohol over Perlite Supported Sulfated Zirconia Catalyst. *Sustainability* **2022**, *14*, 5149. https://doi.org/10.3390/su14095149

Academic Editor: Munjed A. Maraqa

Received: 13 February 2022
Accepted: 22 April 2022
Published: 24 April 2022

1. Introduction

Perlite is a naturally occurring amorphous silica-alumina enriched material with a reported particle diameter between 0–3 mm, low bulk density, and high surface area [1]. Owing to the aforementioned properties, perlite finds potential applications in adsorption [2], as fillers [3], construction and building materials [4], geo-polymerization [5], agriculture industries [6], poultry compost handling [7], medical field [8], etc. The floatable, inert, porous, concentric layered structure of perlite can be conveniently activated and modified by applying different activation techniques. Hence, in recent years, perlite was also utilized as an effective substrate in the synthesis of heterogeneous acid catalysts in different organic transformations, i.e., Fenton reactions of organic compounds [9], the production of aryl/alkyl methane [10], photocatalysis [11], synthesis of xanthenes [12], transesterification reactions [13], condensation reactions [14], the degradation of azo-dyes [15], hydrogenation reactions [16], etc. We recently reported the synthesis of perlite supported catalysts and their catalytic activities in a series of different types of condensation and esterification reactions [17–19]. Due to its rough surface and low density, relatively low price, stability

in various reaction media, high thermal, chemical, and mechanical stability, perlite acts as suitable support in the development of potential heterogeneous catalysts for catalyzing vapor phase organic transformations at an industrial scale and can replace solid catalysts traditionally used in this field.

The alkylation of isomeric cresols using *tert*-butyl alcohol is an industrially relevant reaction as it produces many important products such as butylated hydroxytoluene, 2-*tert*-butyl-*m*-cresol, 4,6-*di*-*tert*-butyl-*m*-cresol, *tert*-butyl-*m*-cresol, 2-*tert*-butyl-*o*-cresol, etc. which are extensively used in the manufacturing of motor and aviation fuel, insulating oil, natural and synthetic rubber stabilizer, synthetic rubber, perfume fixative, musk ambrette, phenol antioxidants, etc. [20–23]. Such reactions are usually performed over homogeneous catalysts such as $FeCl_3$, BF_3, or $AlCl_3$, etc., which can cause severe environmental issues. To overcome such difficulties, strong solid acids such as cation exchange resins [24], 12-Tungstophosphoric acid/phenol-furfural sulfonic acid resin [25], heteropolyacid-sulfated zirconia catalysts [26], Amberlyst-15 [27], and sulfated zirconia [28] were found to be a possible substitute for homogeneous catalysts. Among these catalysts, zirconia and sulfated zirconia are promising candidates for alkylation reactions due to their superior acidity. Nevertheless, limited surface active sites of these materials [29,30], and their deactivation at high temperature [31], require the design of catalysts that combines super acidic characteristics of zirconia and sulfated zirconia, high surface area, and superior thermal stability. For this purpose, some support materials such as silica [32,33], MCM-41 [34], SBA-15 [35], HMS [36], zeolites [37], Al_2O_3 [38], and other waste-derived materials such as fly ash [39] and rice husk silica [40], etc. are used over a period of time, although perlite has never been reported as a support to produce such super solid acid catalysts. In the present work, *tert*-butyl alcohol is taken as an alkylating agent, which generates water as a side product showcasing a greener side of the process. Moreover, in the present work, the alkylation reaction was performed in a vapor phase reaction medium which is quite advantageous in terms of the formation of a lower % of minor and by-products and the enhancement in reaction rates due to the high adsorption of reactants and diffusion of products on catalytic active sites. This increases the yield % and selectivity % of desired products, increases the conversion % of the reactants to many folds, and thus makes the overall process speedy, economical, and energy efficient.

Given that perlite is proven as an efficient support material in the development of easily reusable, solid catalysts, in this perspective, we are now investigating the synthesis and characterization of perlite-supported sulfated zirconia catalysts (SZP) and the analysis of their catalytic activity through the vapor phase alkylation of isomeric cresols with *tert*-butyl alcohol. Different wt. % of sulfated zirconia is loaded on thermally activated perlite through a two-step sol-gel methodology. While several methods are reported for the synthesis of supported sulfated zirconia catalysts, here, the sol-gel method was used to obtain better control of the grain size and porosity [41]. Higher conversion and selectivity % of products reflect the stability of sulfated zirconia on the perlite surface, responsible for the generation of significant acidity and excellent catalytic activity under vapor phase reaction conditions. As-prepared catalysts were found to be more efficient and recyclable when compared with commercially used super acids as well as previously documented solid catalysts used in various alkylation reactions. To the best of our knowledge, no literature was reported on the vapor phase alkylation of isomeric cresols with *tert*-butyl alcohol over perlite-based solid acid catalysts. A further objective of this work is to develop an economical, solid acid catalyst system from silica enriched waste-perlite which can withstand their super acidic sites under the severe reaction conditions of vapor phase reaction medium, possess higher catalytic potential and selectivity towards the formation of the desired products, can be efficiently recovered from the reaction medium and recycled up to many reaction cycles, and could be suitably used in various organic reactions at bulk industrial scale and mitigate the environmental implications of inadequate perlite waste disposal.

2. Materials and Methods

2.1. Materials

Zirconium propoxide was purchased from Sigma Aldrich. Concentrated H_2SO_4, n-propanol, n-butylamine, toluene, methyl orange, *tert*-butyl alcohol, and *o*-, *m*-, *p*- cresols were purchased from RANKEM, India, and used without further purification. Perlite was supplied by Indica Chem. Ind. Pvt. Ltd., Kotdwar, Uttarakhand, India, and used without further purification.

2.2. Preparation of SZP Catalysts

In this study, a series of catalysts were synthesized via a two-step sol-gel technique by loading zirconia propoxide (used as a precursor for sulfated zirconia) on perlite, producing catalysts with zirconia loadings of 9, 12, and 15 wt. %, denoted as SZP-9, 12, and 15, respectively. In a typical synthesis of SZP-9, 12, and 15 catalysts, initially, perlite is heated at a high temperature (800 °C) and designated as thermally activated perlite (TAP). In the first step, a specific amount of zirconium propoxide (1.44 g for 9 wt. %, 1.92 g for 12 wt. %, and 2.39 g for 15 wt. %) was added to a 100 mL beaker and diluted with 15 mL of n-propanol. Then, 6 g of TAP was added to the mixture and kept under constant stirring for 15 min. Water was added dropwise to the TAP-zirconium propoxide mixture under constant magnetic stirring at room temperature. The resulting gel was aged for 24 h and dried at room temperature, and further dried at 100 °C for 12 h. In the second step, the dried gel was powdered and sulfated with 1 N solution of concentrated H_2SO_4 under stirring for 1 h (15 mL H_2SO_4 solution was taken for sulfation of 1 g powdered dried gel). The sulfated gel was filtered and dried at room temperature and then at 110 °C for 12 h for complete evaporation of water from the gel. After that, all the samples were calcined at 600 °C for 2 h in a muffle furnace under static conditions.

2.3. Characterization Techniques

The effect of the studied parameters on the prepared catalysts was examined by N_2 adsorption–desorption, XRD, FT-IR, and pyridine adsorbed FT-IR, SEM, TEM, SEM-EDX, TGA, and UV-Vis DRS techniques. Surface area and pore size distribution were analyzed by N_2 sorption performed on Quantachrome NOVA 1000e by vacuum degassing the samples at 120 °C for 2 h. The crystallographic features of the samples were analyzed by X-ray diffractometer (Bruker) using CuK_α radiation (λ = 1.5406 Å) in the 5–70° 2 theta angle range. UV-Vis spectra (λ = 200–800 nm) were recorded on a UV-Visible spectrophotometer (Perkin Elmer Lambda 950) equipped with a Harrick diffuse reflectance accessory at ambient temperature. Thermogravimetric analysis was performed on a Mettler Toledo thermal analyzer in N_2 flow with a temperature range of 50–1000 °C and heating rate of 10 °C/min under N_2 flow (50 cm^3/min). The FT-IR study was executed on a Bruker FT-IR Spectrophotometer (TENSOR 27) in DRS (Diffuse Reflectance System) mode by mixing about 100 mg sample with KBr in a 1:20 weight ratio. The spectra were recorded in the range of 4000–550 cm^{-1} with a resolution of 4 cm^{-1}. The acidity of the catalysts was determined by pyridine adsorbed FT-IR. The samples (about 100 mg) were activated at 450 °C for 2 h, cooled at room temperature and saturated with 1.0 mol% pyridine under N_2 flow for 2 h. After the pyridine sorption, the sample was kept at 120 °C under N_2 flow for 90 min to remove physically adsorbed pyridine. The spectra were recorded in the range of 1600–1350 cm^{-1} with a resolution of 4 cm^{-1}. Further, the total acidic content was calculated using the Hammett indicator method [42]. In it, samples were calcined at 450 °C for 1 h before carrying out the indicator tests. A 1.0 N n-butylamine solution was prepared using toluene. In total, 0.1 g of calcined sample was taken, and then 2.5 mL of indicator solution were added (0.1 g of methyl orange indicator in 5 mL of toluene) to the sample suspension and left for 12 h. In this mixture, 1.0 N of n-butylamine in toluene was added from a 50 mL burette until the endpoint was reached. The endpoint was achieved when the red color turned yellow. The products were analyzed by Gas Chromatograph (Agilent Technologies 7820A, with FID and Agilent J&W Advanced Capillary HP 5 GC Columns of 30 m length

and 0.320 mm diameter, programmed oven temperature of 60–325 °C, and N_2 (1.5 mL/min) as a carrier gas. The SEM studies were performed on a JEOL-JSM 5600 instrument at a probe current of 10^{-12}–10^{-6} A and accelerating voltage of 0.5–30 kV, 5 nm resolution, and 125 mm sample size. All samples were examined with a copper coating in high-vacuum mode. A Hitachi (H-7500) instrument with a resolution of 0.36 nm (point to point) with a 40–120 kV operating voltage and magnification up to 6 lakh times in high resolution mode was used. For the analysis of the powders, the samples were prepared through ultrasonic dispersion in acetone, and a drop of the resultant suspension was evaporated and mounted onto carbon-supported grids.

2.4. Catalytic Reactions

The alkylation of *o*, *m*, and *p*-cresols using *tert*-butyl alcohol was conducted in a vapor phase micro-reactor (fabricated by Chemito) shown in Figure 1, consisting of a 4.5 cm long, stainless-steel reactor tube (2.54 cm outer diameter and 2.2 cm of inner diameter) positioned in a furnace with a PID (proportional-integral-derivative) temperature controlling system. Before catalytic reactions, SZP catalysts (0.6 g) were pre-heated at 400 °C for 1 h in an N_2 environment with a heating rate of 10 °C/min. A mixture of reactants (isomeric cresols and *tert*-butyl alcohol) of desired molar ratio along with N_2 gas was first heated, mixed, and then delivered to the reactor tube by a vaporizer and pre-mixer at the appropriate reaction temperature (WHSV = 0.83 h^{-1}). The mass flow controller (SS 316, MFC-101) and a back pressure control valve maintained a consistent flow rate of N_2 gas and set pressure conditions, respectively. After passing through the catalyst bed, the reaction mixture was cooled (ice trap) to room temperature and samples were collected every hour. The effluent (product vapors) accumulated in a gas–liquid separator made up of stainless steel was cooled down by passing through a water condenser after every hour and analyzed by a gas chromatograph. All the experiments were replicated three times with each variable.

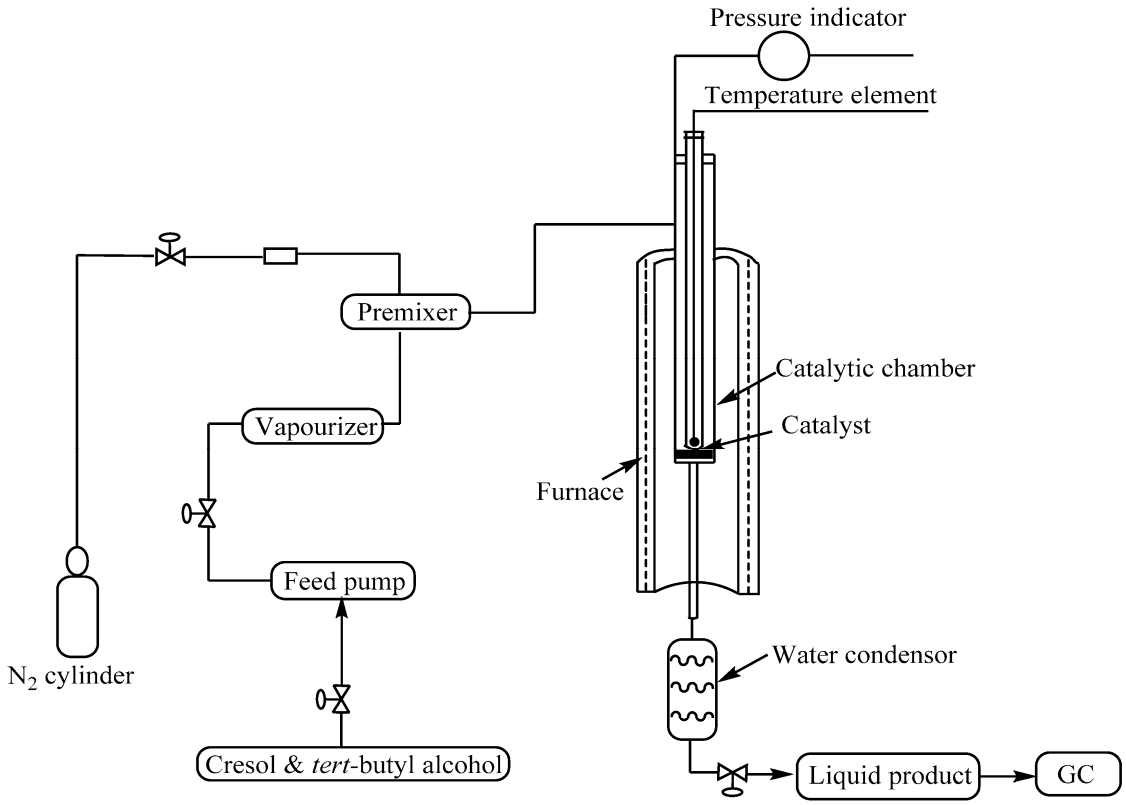

Figure 1. Schematic representation of vapor phase reactor used for alkylation of isomeric cresols by *tert*-butyl alcohol.

Conversion, selectivity %, mass balance closure and WHSV were calculated using the following formulae:

$$Conversion\ \% = \frac{Mass\ of\ reactant\ reacted}{Mass\ of\ reactant\ fed} \quad (1)$$

$$Selectivity\ \% = \frac{Mass\ of\ desired\ products\ formed}{Mass\ of\ total\ products\ formed} \quad (2)$$

$$WHSV = \frac{Flow\ of\ reactants}{Mass\ of\ catalyst} \quad (3)$$

$$m_b = \frac{m_{fed}}{m_{outlet}} \quad (4)$$

where m_b (%) is the mass balance closure in percent, m_{fed} is the total mass of reactants fed into the reactor, and m_{outlet} is the total mass of products and unreacted reactants at the outlet of the reactor (measured using the GC).

3. Results

3.1. Characterization

The surface modification of perlite by sulfated zirconia was evaluated by N_2 adsorption–desorption. Table 1 show an approximately constant increase in specific surface area with increasing sulfated zirconia loading with a maximum area of 80 m^2/g for the SZP-15 catalyst. Zirconia itself possesses a lower specific surface area [43], which increases sulfation due to the interaction between sulfate and zirconium ions. Sulfation resists sintering, and thus the specific surface area of zirconia increases after it [44]. Table 2 summarize different characteristics of the preferred SZP-15 catalyst obtained using different analytical techniques discussed later in this work. The prepared SZP-15 catalyst has well-defined uniform pore dimensions with an average pore volume and pore diameter of 0.03 cm^3/g and 4.8 nm, respectively.

Table 1. BET surface area of perlite and prepared catalysts.

Samples	BET Surface Area (m^2/g)
Perlite	3
TAP	2
SZP-9	49
SZP-12	66
SZP-15	80

Table 2. Surface analysis results of SZP-15 catalyst.

Surface area, S_{BET} (m^2/g)	80
Sulfur content (wt.%)	5.46
Total pore volume, V_p at (p/p_o = 0.95) (cm^3/g)	0.03
Average pore diameter, D_p (nm)	4.8
Crystallite size (nm)	Cannot be measured
Particle size (nm)	9–25

Figure 2a show a broad band centred at 2θ = 10–15°, indicating the presence of amorphous silica [45], while in Figure 2b, a small crystalline peak appears at 2θ = 27.6° showing the presence of quartz crystalline phase [46]. After the incorporation of sulfated zirconia on the TAP surface in SZP-9, 12, and 15 catalysts (Figure 2c–e), monoclinic and tetragonal phases of zirconia could be seen at 2θ = 25–27° and 2θ = 30, 41, 50, and 60°,

respectively (ICSD collection code 066787) [47,48]. On increasing the loading of sulfated zirconia from 9 to 15 wt. %, the intensity for both monoclinic and tetragonal phases also increased. The number of peaks and the intensity of tetragonal phases were found to be highest in the preferred SZP-15 catalyst. In SZP-9 and 12, the sulfate content was relatively lower; hence, the monoclinic phases were stronger and more in number than the tetragonal phases. The crystallite size of tetragonal and monoclinic phases decreased on sulfate ions incorporation in catalysts [49], and thus the size determination of such peaks is not feasible. A hump centred at 2θ = 10–13°, characteristic of amorphous silica of perlite, was retained in the XRD patterns of all samples.

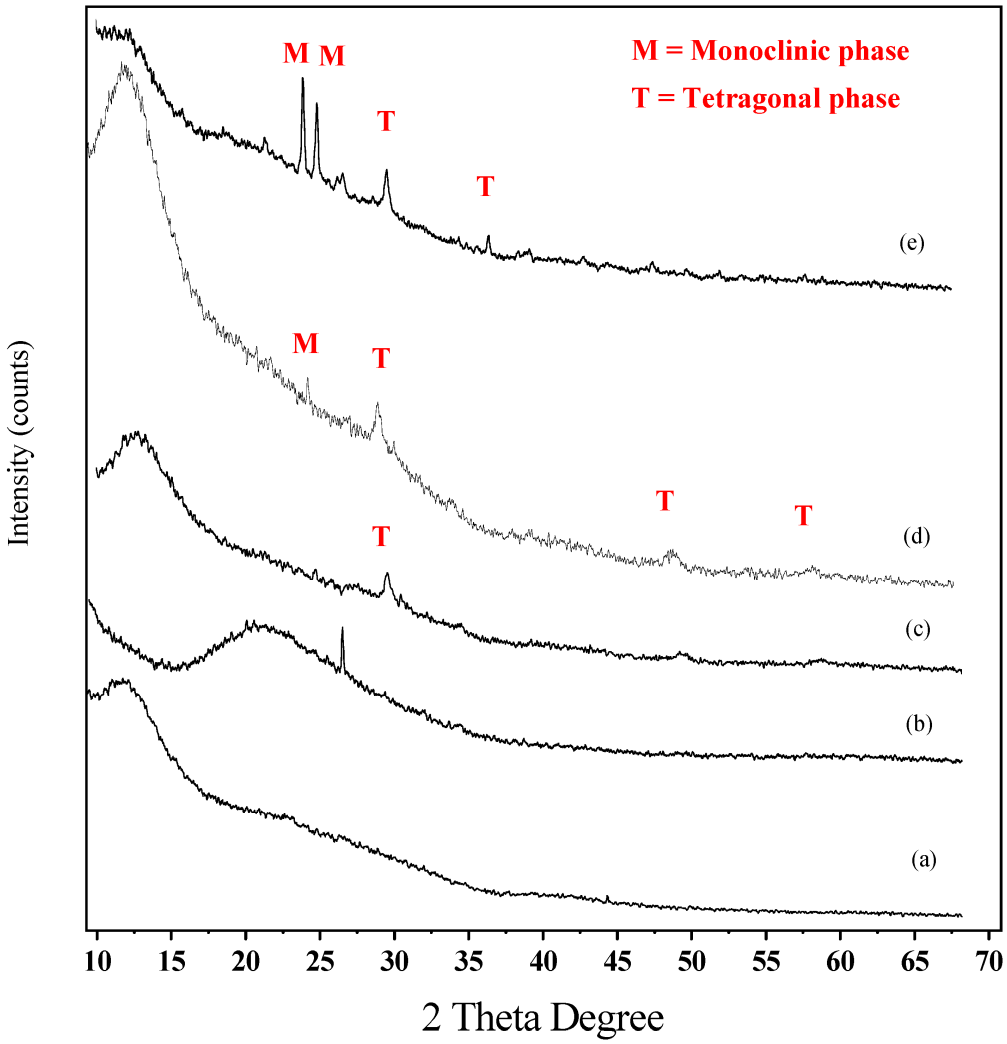

Figure 2. X-ray diffraction pattern of (**a**) Perlite, (**b**) TAP, (**c**) SZP-9, (**d**) SZP-12, and (**e**) SZP-15.

The FT-IR spectra of perlite and TAP, as shown in Figure 3a,b, respectively, are suitably explained in our previous report [17]. The FT-IR spectra of SZP-9, 12, and 15 catalysts, as displayed in Figure 3c–e, show a broad band in the region between 3600–3300 cm^{-1}, characteristic of surface –OH groups whose intensity increases progressively with an increase in loading of sulfated zirconia due to incorporation of zirconia and sulfate content. Broadness in this band is due to the presence of surfacial hydroxyl groups (–Si-OH) with strong intermolecular hydrogen bonding and physisorbed water molecules, which decreases in the case of TAP, conferring water loss on thermal activation [17]. A peak around 1630 cm^{-1} is also observed in all samples, corroborating the bending mode ($\delta_{O\text{-}H}$) of the –OH groups and water molecules [50]. The persistence of these bands in all catalysts even after calcination at 550 °C points out the stability of their Brønsted acidity.

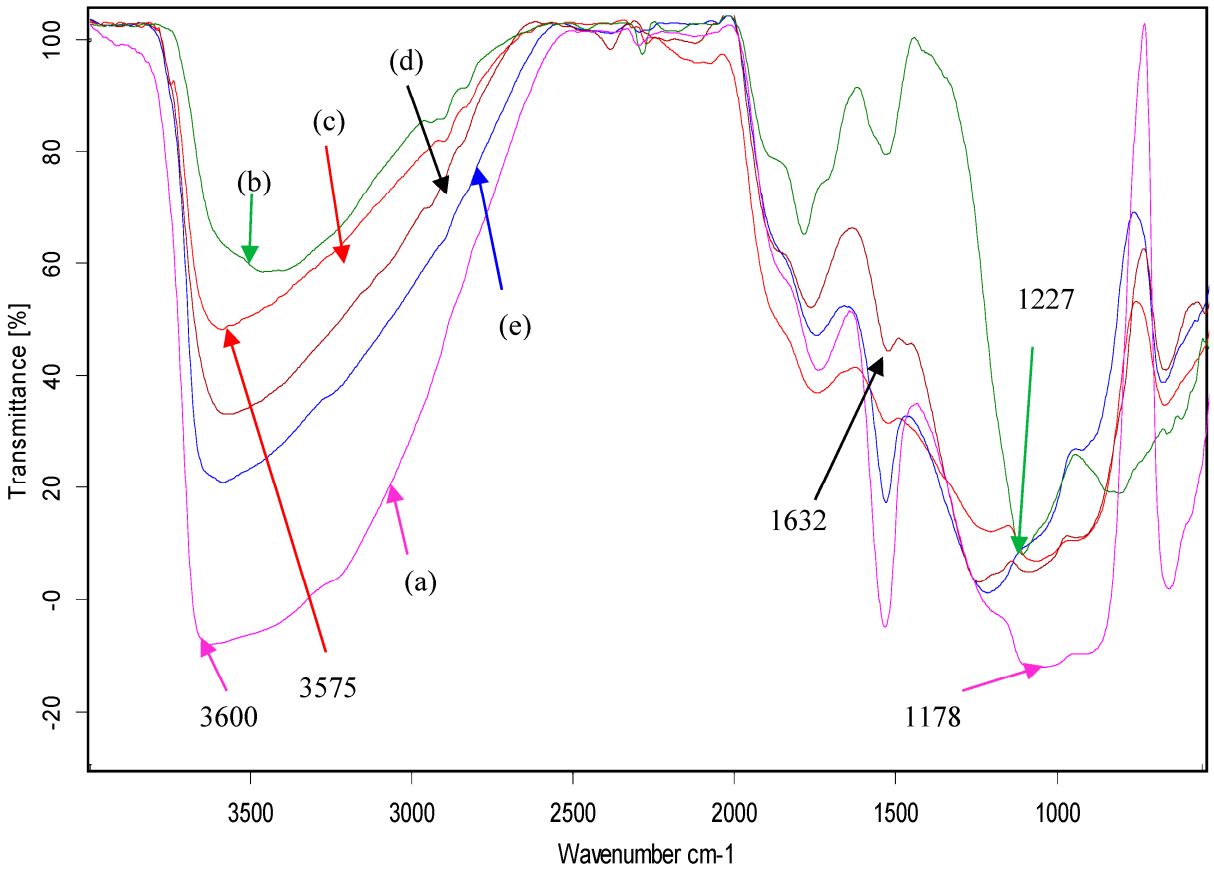

Figure 3. FT-IR spectra of (**a**) Perlite, (**b**) TAP, (**c**) SZP-9, (**d**) SZP-12, and (**e**) SZP-15.

A characteristic band of S=O asymmetric stretching vibration 1391–1382 cm^{-1} [39] shifts towards a lower wavenumber, 1344 cm^{-1} here, which corresponds to a partial ionic character of S-O bonds responsible for increased Bronsted acidity in SZP catalysts [51]. The absence of a band around 1400 cm^{-1} in all the catalysts indicates the absence of polynuclear sulfates, $S_2O_7^{-2}$ [52]. In addition to zirconium, the Si-O-Si lattice stretching vibration appearing in the 1300–1100 cm^{-1} region shifts to lower wavenumbers, i.e., 953 and 898 cm^{-1}, probably due to the incorporation of zirconium ions into the silica network of perlite [53] and the formation of Zr-O-Si linkage [54]. The intensity of these bands increases progressively with an increase in zirconium content from SZP-9 to SZP-15 catalysts. Some bands in the region of 700–550 cm^{-1} can be attributed to Zr-O stretching vibrations, which are still less resolved due to their superimposition with Si-O-Si deformation bands [34].

The acidity of perlite, TAP, and catalysts was determined using pyridine adsorption in conjunction with FT-IR spectroscopy (Figure 4). Broad and less intense bands centered at 1550 cm^{-1} as seen in spectra of perlite and TAP (Figure 4a,b) indicate the co-ordinate bonding of pyridine with surficial -OH groups. The absence of bands around 1540 and 1440 cm^{-1} reveals no sign of Bronsted and Lewis acidity in perlite and TAP [55]. The Bronsted acidic sites were obtained at 1545 cm^{-1}, whereas the Lewis acidic sites were obtained at 1445 cm^{-1} [56–59]. After an increase in sulfur content, the number of Lewis and Brønsted acid sites also increased [60]. The stability of the tetragonal phase also plays an important role in the increase in Brønsted acid sites as it produces the most stable structure during hydration [61]. Thus, Brønsted bands are broader in SZP-9 and 12 and sharper in SZP-15, while Lewis bands are more intense and broader in SZP-12 and 15 and less intense in SZP-9. A band present at 1485 cm^{-1} in all samples was ascribed to the presence of both Brønsted and Lewis sites in the samples [55]. Sulfate groups possess an -I effect and withdraw the electron density from zirconia, thus creating Lewis acidic sites there, while protons formed by these sulfate groups create Bronsted acidic sites. Since both sulfur

and zirconia content is increasing from SZP-9 to 15, the concentration of both acidic sites is increasing in the same trend and in accordance with our previous report [39].

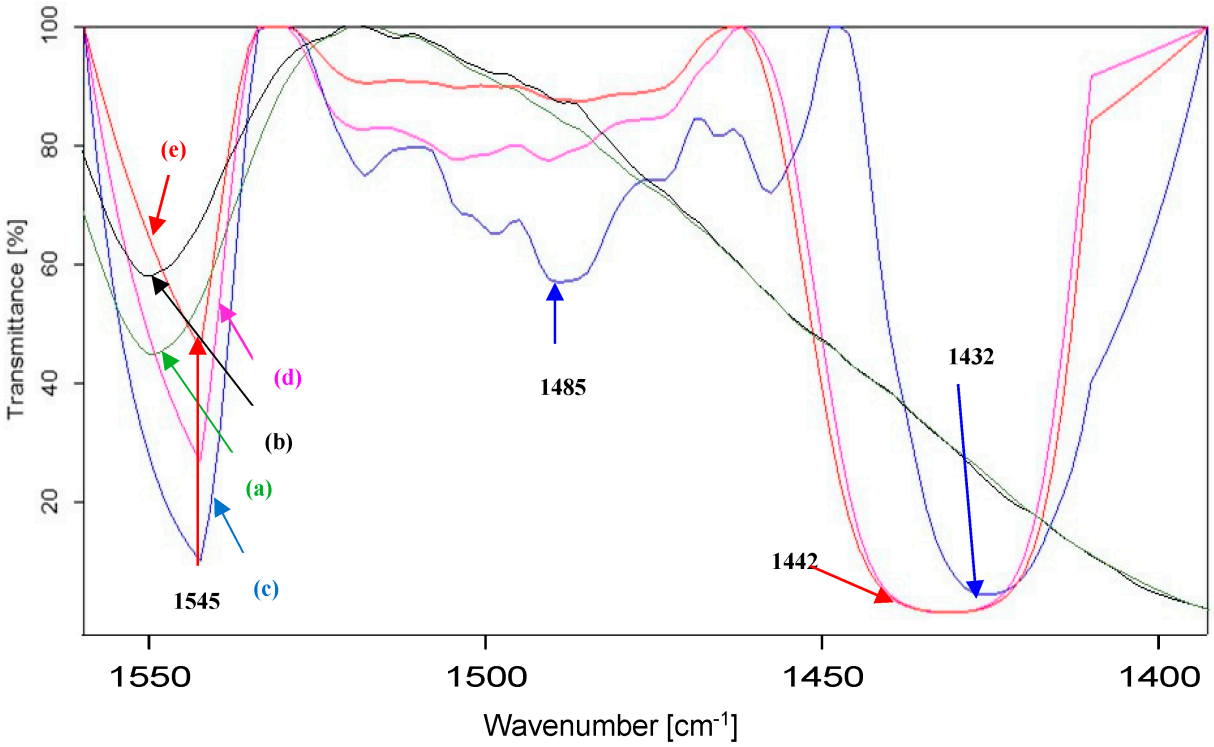

Figure 4. Pyridine adsorbed FT-IR spectra of (**a**) Perlite, (**b**) TAP, (**c**) SZP-9, (**d**) SZP-12, and (**e**) SZP-15.

Total acidic content was determined for all samples using the Hammett indicator method as described earlier in the 'Characterization techniques' section. With perlite and TAP, there was no color change and the endpoint was not achieved; hence, it can be concluded that perlite and TAP are chemically inert in nature, with negligible acidic sites. The acidic strength of SZP catalysts was found to be in the order—$3.0 < H_0 < 4.8$. The total acid amount of SZP-9, 12, and 15 was found to be 0.7, 1.0, and 1.4 mmol/g, respectively.

The SEM micrograph of perlite (Figure 5a) reveals the irregular, layered morphology of its particles, while the SEM image of SZP-15 (Figure 5b) depicts the agglomeration of amorphous particles after sulfation with H_2SO_4. Shiny flakes show the presence of zirconia on the surface of perlite. The elemental composition of perlite and SZP-15 was confirmed by SEM-EDX analysis (Table 3). It showed that silica and alumina are the major constituents of perlite. The presence of S and Zr in all catalysts confirms the loading of sulfated zirconia, which increases on increasing S and Zr content in SZP-9, 12, and 15 catalysts. The leaching of minor constituents such as K, Zn, and Fe indicates effective sulfation with H_2SO_4.

The TEM image of perlite (Figure 6a) exhibits its irregular morphology. The dark field image of the SZP-15 catalyst (Figure 6b) shows small dots indicating the presence of nanocrystalline, aggregated tetragonal zirconia particles dispersed on the perlite surface [62]. With the help of another TEM image (Figure 6c), the particle size of the catalyst was determined, which was found to be in the nano range of 9–25 nm. Both TEM images conclude that the catalyst particle size is heterogeneous, with particles $\geq$ 100 nm and particles in the 9–25 nm range. These TEM images also support the fact that on sulfation, the size of the zirconia particles decreases, thus enhancing the surface area of the final catalyst [63].

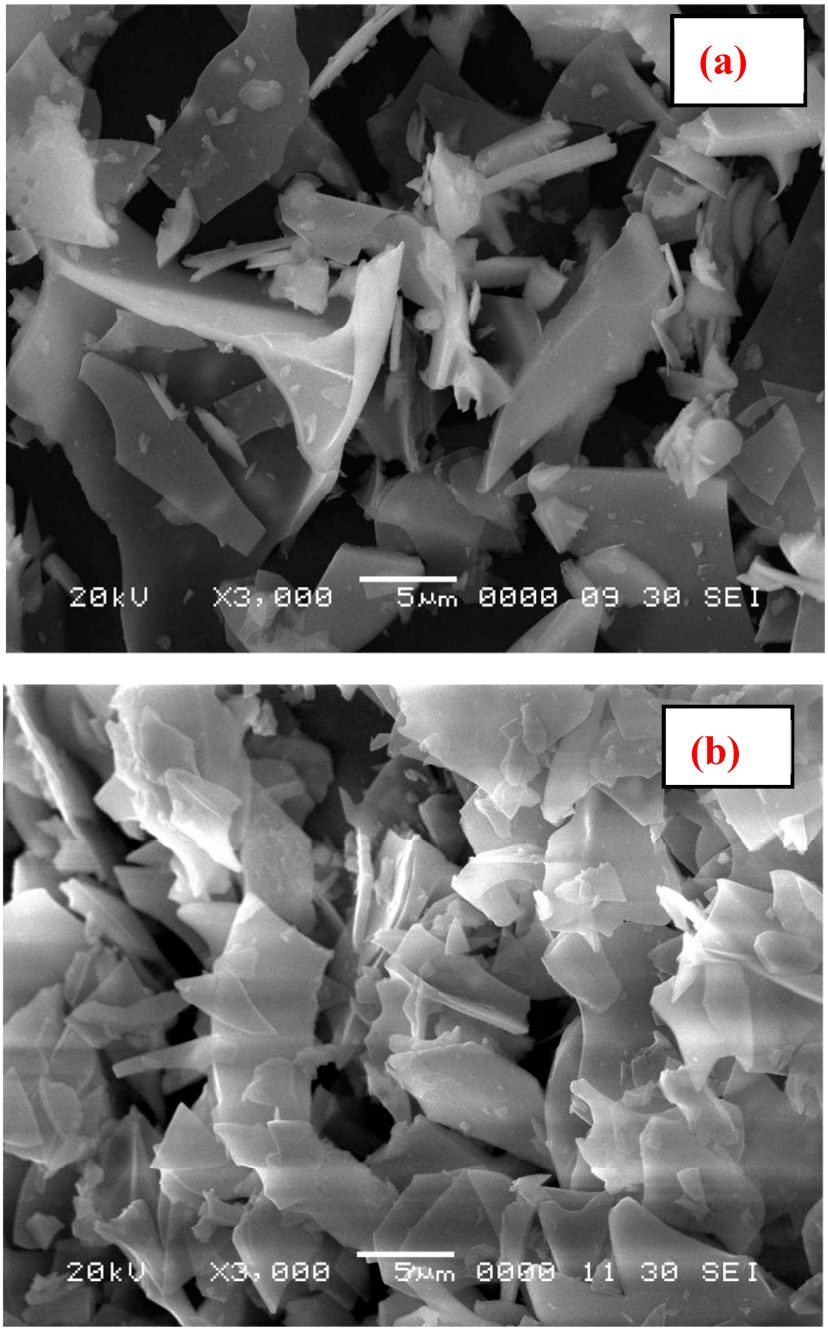

Figure 5. SEM micrographs of (**a**) Perlite and (**b**) SZP-15.

Table 3. EDX analysis of perlite, SZP-9, SZP-12, and SZP-15.

Samples	SiO_2 (wt%)	Al_2O_3 (wt%)	K_2O (wt%)	Na_2O (wt%)	ZnO (wt%)	FeO (wt%)	TiO_2 (wt%)	SO_3 (wt%)	ZrO_2 (wt%)
Perlite	72.74	14.79	7.02	2.10	2.04	0.91	0.40	-	-
SZP-9	77.27	16.64	-	1.40	-	-	0.40	1.31	2.98
SZP-12	74.51	16.63	-	1.67	-	-	0.32	1.24	5.63
SZP-15	69.71	14.45	-	1.83	-	-	-	2.03	11.98

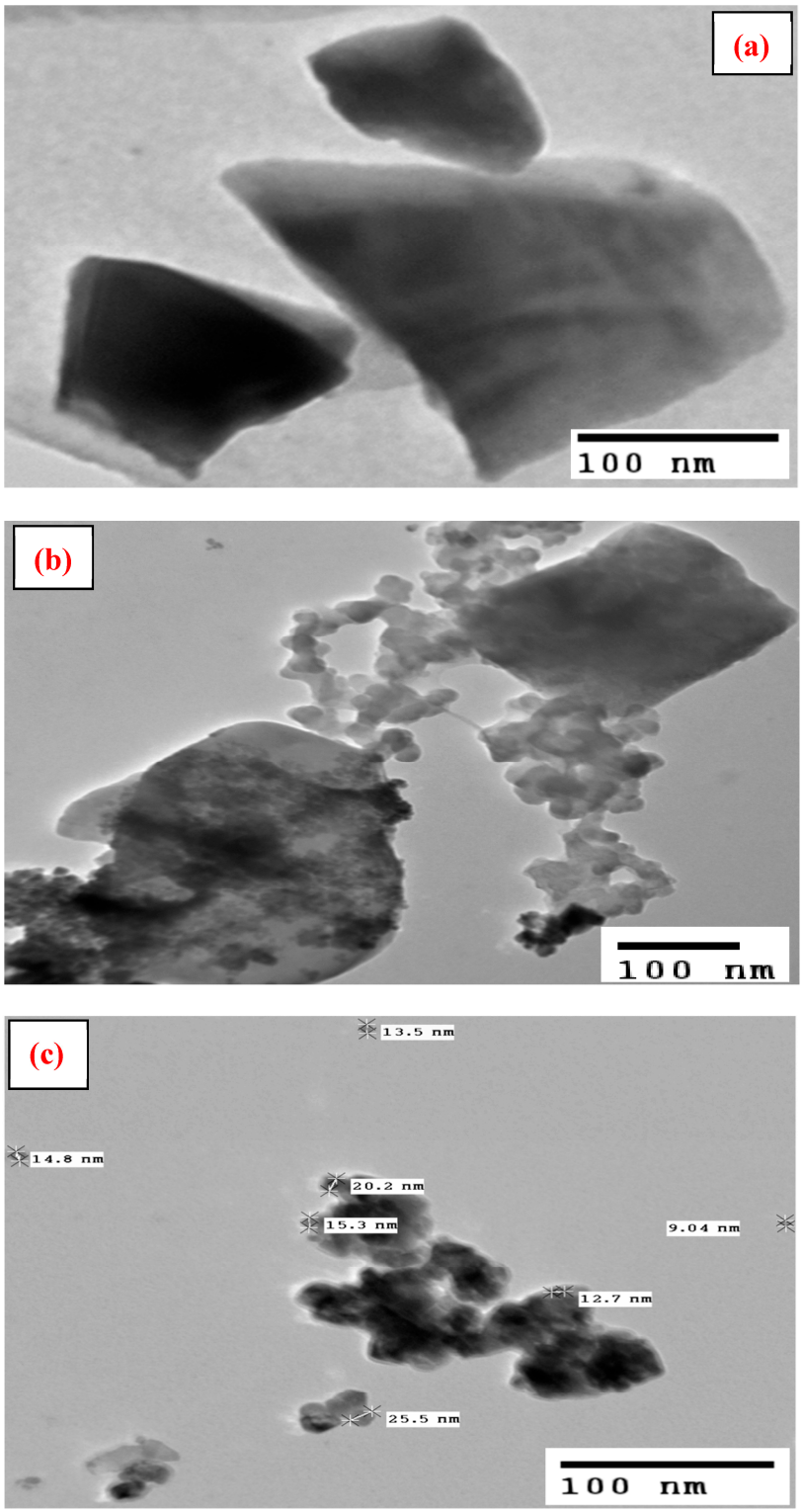

Figure 6. TEM micrographs of (**a**) Perlite, (**b**,**c**) SZP-15.

The TGA curve of perlite (Figure 7) depicts a sharp weight loss in the range of 100–400 °C, which could be due to the removal of adsorbed water on the surface. At a higher temperature, a gradual weight loss is seen, which can be due to the decomposition of volatile metal oxides or carbonaceous materials present in perlite. In the TGA pattern of the SZP-15 catalyst, as displayed in Figure 7, the initial sharp weight loss up to 400 °C could be assigned to the elimination of the physically adsorbed water of hydration. A

gradual weight loss in a higher temperature range, i.e., 600–900 °C, can be due to the decomposition of sulfate ions and the transformation of tetragonal to the monoclinic phase of zirconia. The overall weight loss of SZP-15 is lower than the weight loss of the perlite only for temperatures greater than 200 °C, and its total weight loss is much less than the unsulfated materials suggesting that sulfate species displaced some loosely bonded surface hydroxyl groups [64]. Figure 8, showing the change in slope of both curves (dm/dT, m is the catalyst mass, and T the temperature) as a function of temperature, presents a clearer picture of weight loss throughout the whole temperature range.

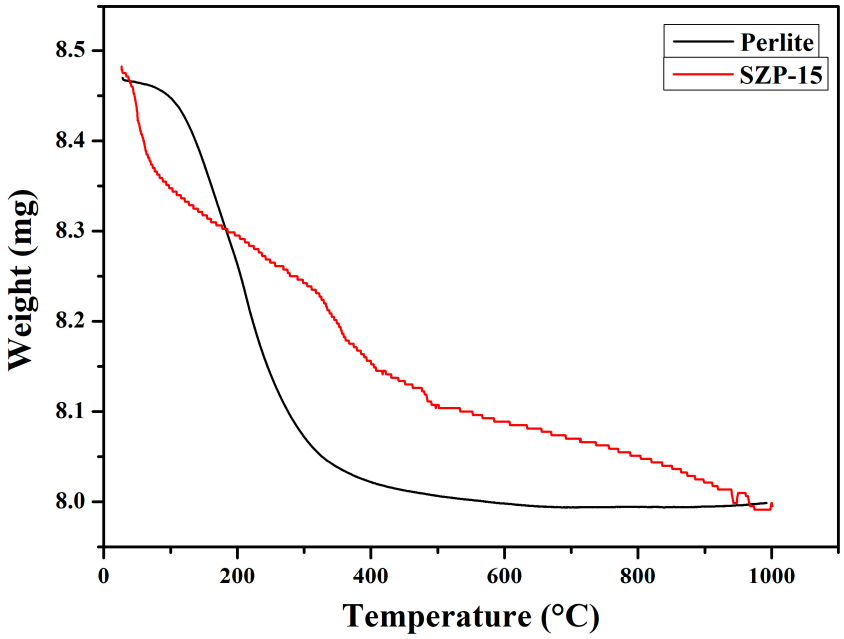

Figure 7. TGA curves of perlite and SZP-15.

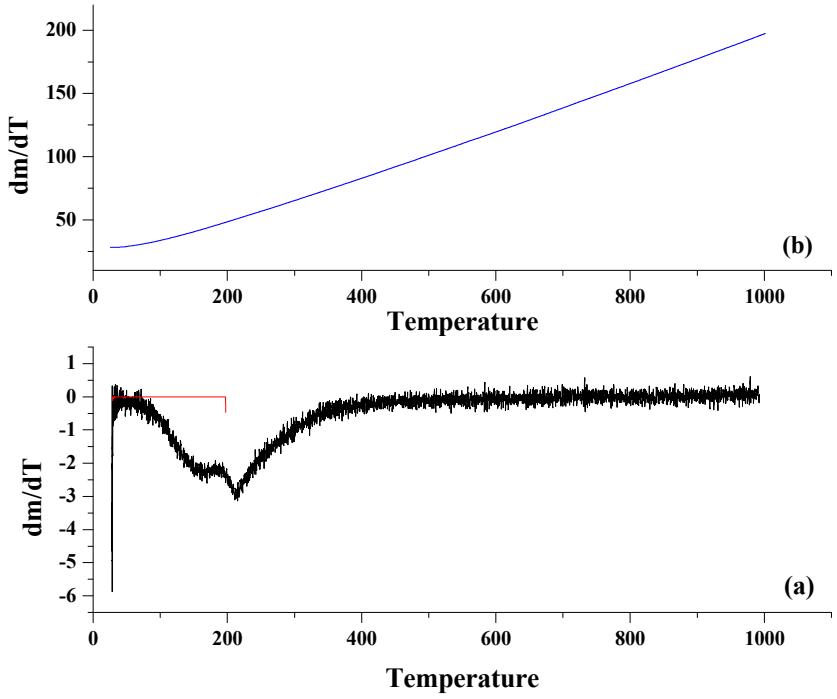

Figure 8. dm/dT curve of (**a**) Perlite and (**b**) SZP-15.

The UV-Vis DRS spectrum of perlite (Figure 9) shows a broad band around 230 nm which is usually observed in aluminosilicates [65]. It accounts for the presence of silica; however, it does not help in differentiating the nature of silica as such kind of band can be seen in both amorphous and crystalline silica compounds such as silica gel, zeolites, etc. In the UV-Vis spectra of all the catalysts (Figure 9), a band near 210 nm is seen, which can be assigned to oxygen–zirconium charge transfer [66]. It also suggests the presence of the tetragonal phase of ZrO_2 in a tetrahedral environment. Such bands are seen when zirconium species are successfully incorporated into the mesoporous silica skeleton of support. The absence of a band at 230 nm in all catalysts reveals the non-dominance of the monoclinic phase of ZrO_2 [53]. For nano sulfated zirconia particles, an additional band at 298 nm attributing to oxygen–zirconium charge transfer should also appear, which is present in all catalysts [67]. A band of 375–400 nm, characteristic of rich zirconium content, is also present in all catalysts.

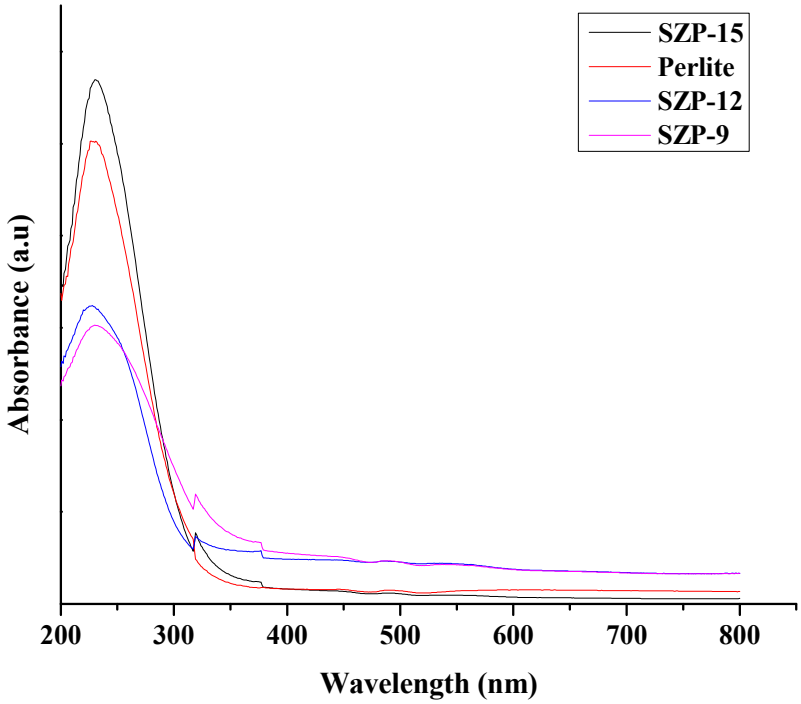

Figure 9. UV-Vis DRS spectra of perlite, SZP-9, 12, and 15.

3.2. Catalytic Reaction

The results of the alkylation test reaction between *p*-cresol and *tert*-butyl alcohol over the SZP catalyst are depicted in Table 4. The results show that no reaction occurs in the absence of a catalyst; in addition, perlite and TAP also show negligible catalytic activity. SZP-9 and 12 show less catalytic activity towards the reaction, while SZP-15 shows the maximum conversion % owing to the presence of sufficient surface-active sites, as confirmed by the pyridine-adsorbed FT-IR studies. Acidity measurement results obtained from the Hammett indicator and pyridine adsorbed FTIR confirm the chemically inert nature of perlite and TAP, so they gave negligible conversion in the test reaction. SZP-15 is a superacid catalyst, i.e., a combination of both Bronsted and Lewis acidic sites, and both types of sites may take part in the alkylation of cresols with *tert*-butyl alcohol. Both the factors, the acidic content of prepared catalysts and the increase in their surface area, play a significant role in catalytic activity.

To achieve the maximum conversion and selectivity % of the desired products, two reaction parameters, temperature and molar ratio, were optimized using a SZP-15 catalyst. The optimized reaction conditions were: temperature = 245 °C; molar ratio (*p*-cresol:*tert*-butyl alcohol = 1:1); WHSV = 0.83 h^{-1}; weight of catalyst = 0.6 g.

Table 4. Catalytic performance of different samples for alkylation reaction of *p*-cresol by *tert*-butyl alcohol.

Catalysts	Conversion (%)
Without catalyst	Negligible
Perlite	Negligible
TAP	Negligible
SZP-9	78 ± 1.8
SZP-12	86 ± 0.7
SZP-15	92 ± 0.7

Reaction conditions: Temperature = 245 °C; molar ratio (*p*-cresol:*tert*-butyl alcohol = 1:1); WHSV = 0.83 h^{-1}; weight of catalyst = 0.6 g.

3.2.1. Effect of Reaction Temperature

The alkylation reaction was performed at various temperatures in the range of 195–285 °C. In the case of *o*-cresol, there is a probability of the formation of both *ortho* and *para* isomers; however, *ortho*-selectivity is more as only one *ortho* position is available for alkylation. The maximum conversion % of *o*-cresol was attained at 235 °C with 95% selectivity towards the formation of 6-TBOC (Table 5). The effect of temperature variation on the alkylation of *m*-cresol is summarized in Table 6. Here, except for intermediate TBMCE, two main products were obtained: 6-TBMC and 4,6-DTBMC, along with a minor quantity of 4-TBMC. At 245 °C, the selectivity towards 6-TBMC formation reached 100%, with the highest % conversion of *m*-cresol (98%). Since the second and fourth positions on *m*-cresol are more sterically hindered, they are less favoured for electrophilic attack by *tert*-butyl cation, resulting in *tert*-butylation at the sixth position and 100% selectivity towards the formation of 6-TBMC. Table 7 demonstrate the effect of temperature on the conversion % of *p*-cresol and the distribution of liquid products obtained during alkylation with *tert*-butyl alcohol. The products of the reaction consist of 2-TBPC, 2,6-DTBPC as well as TBPCE. In the case of *p*-cresol, both *ortho*-positions are comparable, and after the bonding of the first alkyl group to the cresol ring, its nucleophilicity increases which leads to the formation of a considerable amount of *di*-*tert*-butylated product as compared with alkylation of other isomeric cresols with *tert*-butyl alcohol. During the alkylation of all isomeric cresols with *tert*-butyl alcohol in the presence of SZP-15, on increasing the reaction temperature, the conversion % of cresols initially increased and then declined after attaining maxima. This may be due to the de-alkylation of the alkylated products at a higher temperature. In all these reactions, C-alkylation predominates over O-alkylation owing to optimum acidic sites on the surface of SZP-15, as less acidic catalysts support O-alkylation to give ether as the main product [26].

3.2.2. Effect of Molar Ratio

The correlation between the molar ratio of isomeric cresols:*tert*-butyl alcohol on the conversion % of cresols and product selectivity % was studied by carrying out reactions at varying molar ratios ranging from 1:1 to 3:1 over SZP-15 catalyst. Table 8 show that the maximum conversion % of *o*-cresol was attained at an *o*-cresol:*tert*-butyl alcohol molar ratio of 1:2. On further increasing the concentration of *tert*-butyl alcohol, the conversion % of *o*-cresol and selectivity % of major products decreased which could be due to the steric hindrance of the *tert*-butyl group. The same trend appears on increasing the concentration of another reactant, i.e., *o*-cresol. Thus, it can be concluded that on increasing the concentration of any reactant on the catalyst surface, fewer active sites remain available for the adsorption of another reactant, which decreases the contact between the two reactants and the desired conversion % and product selectivity % cannot be attained. In the case of *m*-cresol, Table 9 reveal that at *m*-cresol:*tert*-butyl alcohol molar ratio 1:2, the highest % conversion of *m*-cresol was obtained. Again, on increasing the concentration of any reactant, conversion and selectivity % decrease. Table 10 show that the conversion of *p*-cresol was highest at a *p*-cresol:*tert*-butyl alcohol molar ratio of 1:1 and then decreased with a further increase

in the concentration of reactants. In the case of *m*-cresol and *p*-cresol, the selectivity % of *di*-*tert*-butylated products, 2,6-DTBMC and 2,6-DTBPC, increased due to the increasing concentration of *tert*-butyl alcohol, which may be due to more resident time of the mono-*tert*-butylated product on the catalyst surface. It also causes *di*-*tert*-butylation with the *tert*-butyl carbocation already generated on the catalyst surface.

Table 5. Alkylation of *o*-cresol with *tert*-butyl alcohol over SZP-15 catalyst (*o*-cresol:*tert*-butyl alcohol = 1:2).

Reaction Temperature (°C)	Conversion (%) of *o*-Cresol	m_b (%)	Product Selectivity (%)		
			6-TBOC	4-TBOC	4,6-DTBOC
195	59 ± 0.7	97	83 ± 0.3	13 ± 0.15	04
215	75 ± 0.7	96	90 ± 0.3	09 ± 0.3	01
235	94 ± 0.7	95.2	95 ± 0.06	05	-
255	88 ± 0.8	95.5	95 ± 0.3	05	-
275	83 ± 0.3	95.7	92 ± 0.3	08 ± 0.4	-

Reaction conditions: Molar ratio (*o*-cresol:*tert*-butyl alcohol = 1:2); WHSV = 0.83 h^{-1}; weight of catalyst = 0.6 g.

Table 6. Alkylation of *m*-cresol with *tert*-butyl alcohol over SZP-15 catalyst (*m*-cresol:*tert*-butyl alcohol = 1:2).

Reaction Temperature (°C)	Conversion (%) of *m*-Cresol	m_b (%)	Product Selectivity (%)		
			6-TBMC	4,6-DTBMC	4-TBMC
205	70 ± 0.3	98.9	88 ± 0.3	10 ± 0.15	02
225	85 ± 0.3	98.8	92 ± 0.1	06 ± 0.06	02
245	98 ± 0.7	98.3	100 ± 0.05	-	-
265	90 ± 0.7	98.6	100 ± 0.06	-	-
285	88 ± 0.7	98.6	95 ± 0.3	05	-

Reaction conditions: Molar ratio (*m*-cresol:*tert*-butyl alcohol = 1:2); WHSV = 0.83 h^{-1}; weight of catalyst = 0.6 g.

Table 7. Alkylation of *p*-cresol with *tert*-butyl alcohol over SZP-15 catalyst (*p*-cresol: *tert*-butyl alcohol = 1:1).

Reaction Temperature (°C)	Conversion (%) of *p*-Cresol	m_b (%)	Product Selectivity (%)		
			2-TBPC	2,6-DTBPC	TBPCE
205	71 ± 0.8	98.3	90 ± 0.1	07 ± 0.4	03
225	83 ± 0.7	97.8	89 ± 0.1	08 ± 0.15	03
245	92 ± 0.6	97.9	98 ± 0.05	02	-
265	85 ± 0.7	97.4	90 ± 0.1	10 ± 0.3	-
285	79 ± 0.3	97.6	90 ± 0.1	10 ± 0.3	-

Reaction conditions: Molar ratio (*p*-cresol:*tert*-butyl alcohol = 1:1); WHSV = 0.83 h^{-1}; weight of catalyst = 0.6 g.

Table 8. Correlation between molar ratio of *o*-cresol:*tert*-butyl alcohol, *o*-cresol conversion %, and product selectivity % over SZP-15 catalyst.

Molar Ratio	Conversion (%) of *o*-Cresol	m_b (%)	Product Selectivity (%)		
			6-TBOC	4,6-DTBOC	4-TBOC
1:1	80 ± 0.7	95.9	85 ± 0.1	13 ± 0.5	02
1:2	95 ± 0.6	96.5	95 ± 0.05	05	-
1:3	78 ± 0.8	97.7	88 ± 0.1	10 ± 0.1	02
1:4	68 ± 0.9	98	72 ± 0.15	20 ± 0.3	08 ± 0.1
2:1	86 ± 0.7	97.2	90 ± 0.06	07 ± 0.1	03

Reaction conditions: Reaction temperature = 235 °C; WHSV = 0.83 h^{-1}; weight of catalyst = 0.6 g.

Table 9. Correlation between molar ratio of *m*-cresol:*tert*-butyl alcohol, *m*-cresol conversion %, and product selectivity % over SZP-15 catalyst.

Molar Ratio	Conversion (%) of *m*-Cresol	m_b (%)	Product Selectivity (%)		
			6-TBMC	4,6-DTBMC	4-TBMC
1:1	90 ± 0.6	98.8	90 ± 0.1	04	06 ± 0.03
1:2	96 ± 0.6	98.5	100 ± 0.05	-	-
1:3	88 ± 0.6	98.3	90 ± 0.1	08 ± 0.06	02
1:4	54 ± 0.7	98.7	78 ± 0.1	18 ± 0.1	04
2:1	72 ± 0.8	98.5	84 ± 0.1	09 ± 0.2	07 ±0.3

Reaction conditions: Reaction temperature = 245 °C; WHSV = 0.83 h^{-1}; weight of catalyst = 0.6 g.

Table 10. Correlation between molar ratio of *p*-cresol:*tert*-butyl alcohol, *p*-cresol. Conversion %, and product selectivity % over SZP-15 catalyst.

Molar Ratio	Conversion (%) of *p*-Cresol	m_b (%)	Product Selectivity (%)		
			2-TBPC	2,6-DTBPC	TBPCE
1:1	92 ± 0.7	98.2	98 ± 0.02	02	-
1:2	83 ± 0.7	98.4	89 ± 0.05	08 ± 0.12	03
1:3	78 ± 0.7	98.8	82 ± 0.06	12 ± 0.08	06 ± 0.1
1:4	52 ± 0.3	98.1	70 ± 0.08	20 ± 0.05	10 ± 0.1
2:1	68 ± 0.8	98.5	78 ± 0.07	14 ± 0.07	08 ± 0.1

Reaction conditions: Reaction temperature = 245 °C; WHSV = 0.83 h^{-1}; weight of catalyst = 0.6 g.

3.2.3. Comparison with Other Reported Catalysts

As depicted in Table 11, SZP-15 is recyclable up to five reaction cycles, giving a higher conversion % of *p*-cresol on alkylation with *tert*-butyl alcohol than some previously documented solid catalysts.

Table 11. Comparison of alkylation of *p*-cresol with *tert*-butyl alcohol over reported catalysts and SZP-15 catalyst.

Catalysts	Conversion (%) of *p*-Cresol in First Reaction Cycle	Conversion (%) of *p*-Cresol in Last Reaction Cycle	Reusability of Catalyst (No. of Runs)	Reaction Medium	References
15% TPA/ZrO_2 [a]	~61	-	-	Vapor phase	[26]
D3-MMT [b]	72.84	49.40	03	Microwave irradiations	[22]
Bronsted acidic ionic liquid (IL-1) [c]	80.7	77.9	05	Conventional (autoclave)	[68]
SZP-15 [d]	92	85	05	Vapor phase	This study

Reaction conditions: [a] Temperature = 130 °C, Molar ratio (*tert*-butyl alcohol:*p*-cresol) = 3:1, LHSV = 4 h^{-1}; [b] Temperature = 100 °C, Molar ratio (*tert*-butyl alcohol:*p*-cresol) = 1:1; [c] Temperature = 70 °C, Molar ratio (*tert*-butyl alcohol:*p*-cresol) = 1:1; [d] Temperature = 245 °C, Molar ratio (*tert*-butyl alcohol:*p*-cresol) = 1:1, WHSV = 0.83 h^{-1}.

Scheme 1, given below, shows the major products of alkylation of isomeric cresols with *tert*-butyl alcohol over SZP catalysts, namely, 6-TBOC (6-*tert*-butyl-*o*-cresol), 4-TBOC (4-*tert*-butyl-*o*-cresol), 4,6-DTBOC (4,6-*di*-*tert*-butyl-*o*-cresol), 6-TBMC (6-*tert*-butyl-*m*-cresol), 4-TBMC (4-*tert*-butyl-*m*-cresol), 4,6-DTBMC (4,6-*di*-*tert*-butyl-*m*-cresol), 6-TBPC (6-*tert*-butyl-*p*-cresol), 2,6-DTBPC (2,6-*di*-*tert*-butyl-*p*-cresol), and TBPCE (*tert*-butyl-*p*-cresol ether).

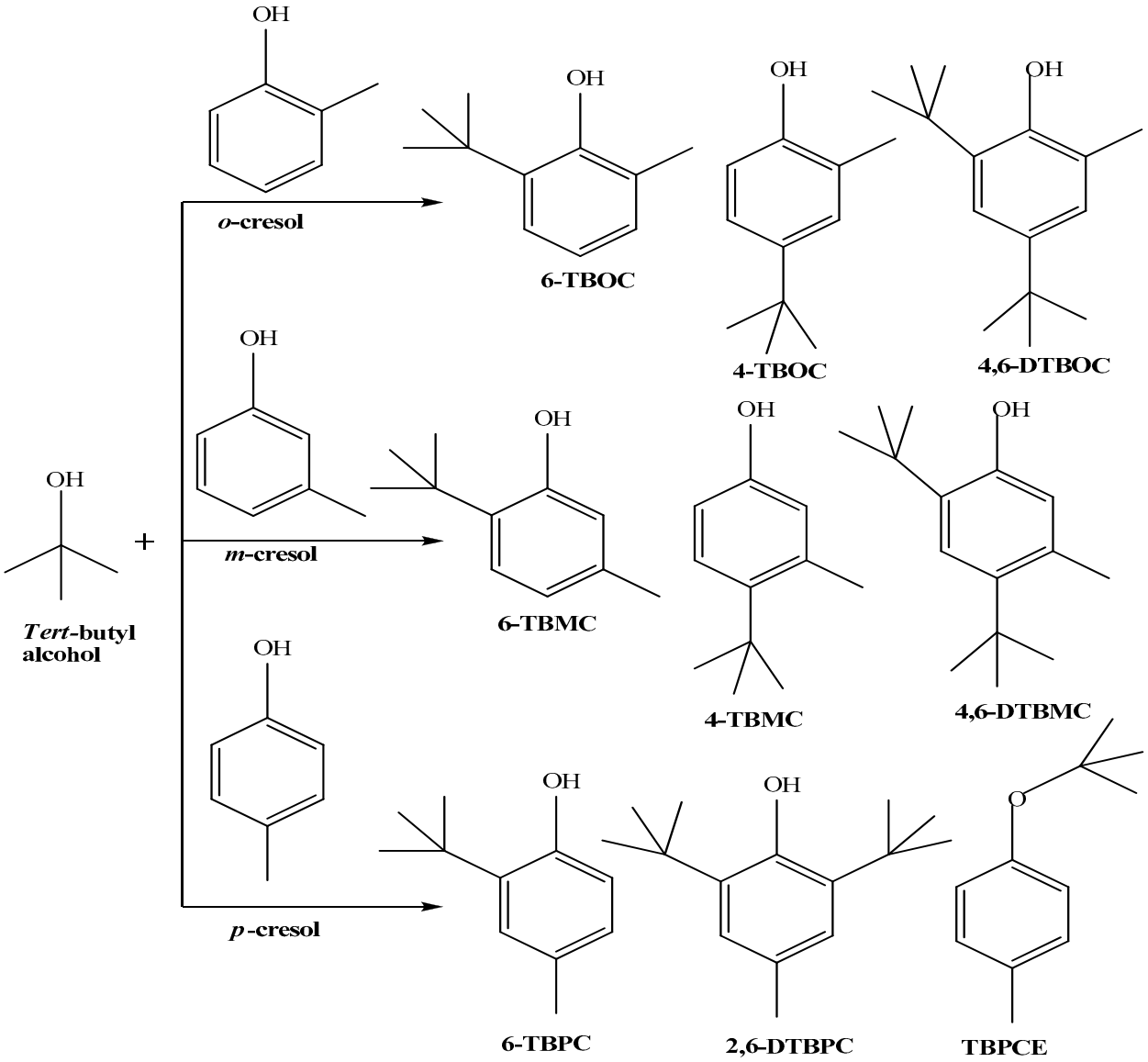

Scheme 1. Major products of alkylation of isomeric cresols with *tert*-butyl alcohol over SZP catalysts.

3.3. Catalyst Reusability

The catalyst was regenerated by passing pure dry air through the catalyst bed at 450 °C for 1 h to check its potential reusability. The reusability results showed that the catalyst could maintain good catalytic performance in the alkylation of *p*-cresol with *tert*-butyl alcohol until the fifth reaction cycle, giving conversion in the range of 92–85% and selectivity in the range of 98–95% of major product, 2-TBPC, as shown in Figure 10. These results are in good agreement with the resemblance of the FTIR spectrum of the fresh SZP-15 catalyst (Figure 11a) with the reused one (Figure 11b). The conversion % was diminished after the fifth reaction cycle, attributed to the physical adsorption of carbonaceous materials on the surface of the SZP-15 catalyst, which blocks the pores of the catalyst, restricts the access of the reactants on catalytic active sites [69,70], limits their reaction with each other, and thus decreases the overall conversion % of the reaction. It was also reflected by the change in color of the SZP-15 catalyst from pale to dark brown color.

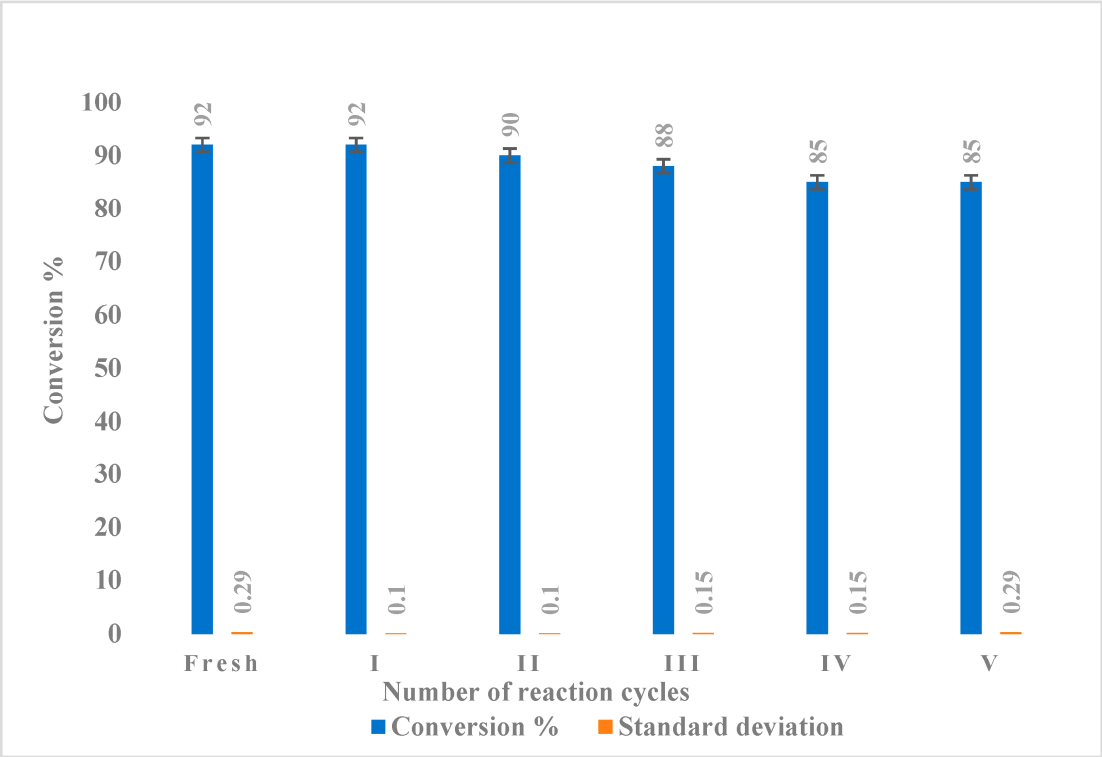

Figure 10. Alkylation of *p*-cresol with *tert*-butyl alcohol over fresh and regenerated SZP-15 catalysts. Reaction conditions: Reaction temperature = 245 °C; WHSV = 0.83 h^{-1}; weight of catalyst = 0.6 g.

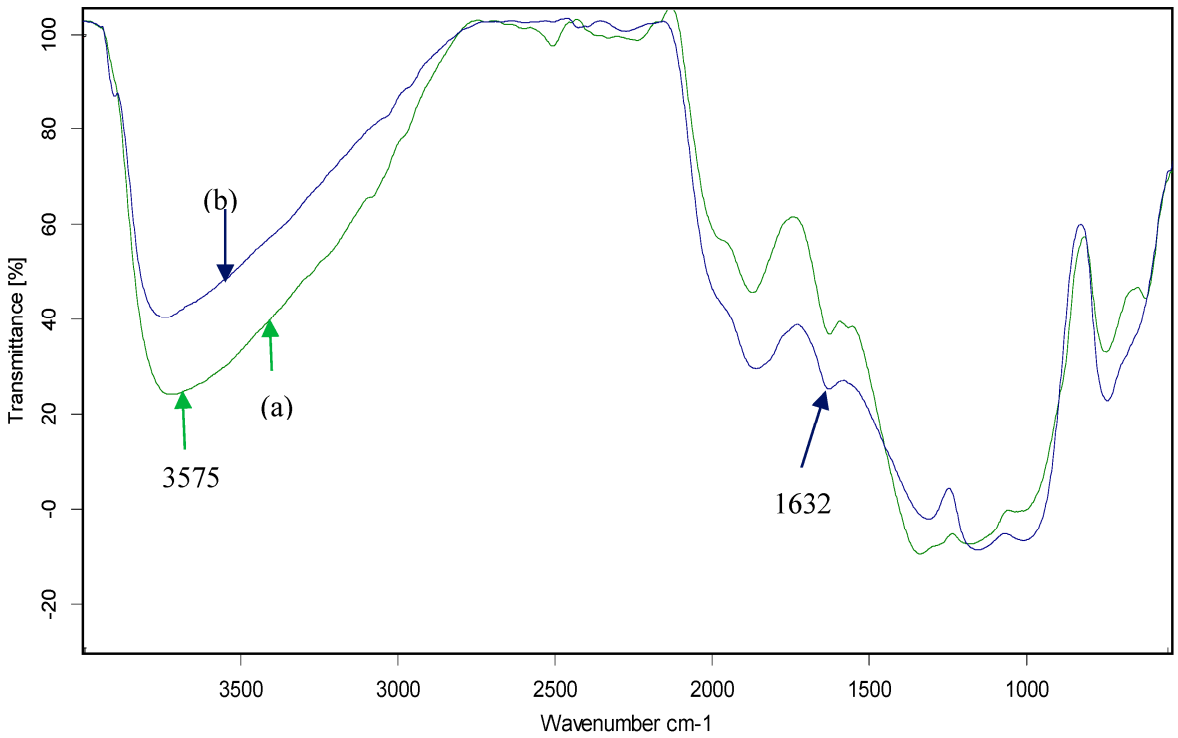

Figure 11. FT-IR spectra of (**a**) fresh and (**b**) SZP-15 catalyst regenerated after 5th run.

4. Conclusions

The present investigation discusses the synthesis of an economical, potential, recyclable solid super acid catalyst-SZP. Thermal activation of perlite stabilizes its rich silica-

alumina content and makes it an excellent support material for further loading of sulfated zirconia in varying amounts through a two-step sol-gel methodology. A SZP-15 catalyst possessing optimum Brønsted and Lewis acidic sites, as determined by pyridine adsorbed FT-IR spectroscopy, efficiently catalyzed the vapor phase alkylation of isomeric cresols by *tert*-butyl alcohol. XRD studies reveal the existence of a catalytic active tetragonal phase of zirconia in SZP-15. The efficiency of the catalyst was further confirmed by the higher conversion % of isomeric cresols and selectivity % of major products obtained in all reactions. In addition, the catalyst can also be reutilized for up to five consecutive reaction runs with analogous potency after simple filtration and thermal treatment. The influence of temperature and molar ratio of reactants were studied during the reactions, which helped in determining the optimized reaction conditions to obtain maximum conversion and selectivity %. The catalytic activity of SZP-15 proved better than some previously reported solid acid catalysts, establishing the stability and recyclability of super acidic sites in the catalyst. Hence, the novelty of this work is that perlite, after its appropriate activation, can replace other conventional supports for the loading sulfated zirconia at a bulk industrial scale and remains highly active under higher temperatures and vapor phase reaction conditions.

Author Contributions: Conceptualization, S.K.M., D.G. and A.R.; methodology, S.K.M.; validation, S.C., S.K. and A.R.; formal analysis, S.K.S.; investigation, S.K.M.; data curation, S.K.S.; writing—original draft preparation, S.K.M. and D.G.; writing—review and editing, S.K.M., D.G. and A.R.; visualization, S.K.M. and D.G.; supervision, A.R. All authors have read and agreed to the published version of the manuscript.

Funding: This research received no external funding.

Institutional Review Board Statement: Not applicable.

Informed Consent Statement: Not applicable.

Data Availability Statement: Data sharing is not applicable.

Acknowledgments: The authors are highly grateful to Indica Chem. Ind. Pvt. Ltd., Kotdwar, Uttarakhand, India, for providing the perlite sample. We are also thankful to Mukul Gupta, Layanta Behera, and T. Shripati, UGC-DAE Consortium for Scientific Research, Indore for XRD and UV-Vis DRS analysis, respectively, the University of Pune for TGA, BET surface area, and SEM and SEM-EDX analysis, and SAIF-Chandigarh for TEM analysis.

Conflicts of Interest: The authors declare no conflict of interest.

References

1. Chakir, A.; Bessiere, J.; Kacemi, K.E.L.; Marouf, B. A comparative study of the removal of trivalent chromium from aqueous solutions by bentonite and expanded perlite. *J. Hazard. Mater.* **2002**, *95*, 29–46. [CrossRef]
2. Koumanova, B.; Peeva-Antova, P. Adsorption of p-chlorophenol from aqueous solutions on bentonite and perlite. *J. Hazard. Mater.* **2002**, *90*, 229–234. [CrossRef]
3. Alihosseini, A.; Taghikhani, V.; Safekordi, A.A.; Bastani, D. Equilibrium sorption of crude oil by expanded perlite using different adsorption isotherms at 298.15 k. *Int. J. Environ. Sci. Technol.* **2010**, *7*, 591–598. [CrossRef]
4. Celik, A.G.; Kilic, A.M.; Cakal, G.O. Expanded perlite aggregate characterization for use as a lightweight construction raw material. *Physicochem. Probl. Miner. Process.* **2013**, *49*, 689–700.
5. Saufi, H.; El Alouani, M.; Alehyen, S.; El Achouri, M.; Aride, J.; Taibi, M. Photocatalytic Degradation of Methylene Blue from Aqueous Medium onto Perlite-Based Geopolymer. *Int. J. Chem. Eng.* **2020**, *2020*, 9498349. [CrossRef]
6. Silber, A.; Bar-Yosef, B.; Levkovitch, I.; Kautzky, L.; Minz, D. Kinetics and mechanisms of pH-dependent Mn(II) reactions in plant-growth medium. *Soil Biol. Biochem.* **2008**, *40*, 2787–2795. [CrossRef]
7. Kalus, K.; Opaliński, S.; Maurer, D.; Rice, S.; Koziel, J.A.; Korczyński, M.; Dobrzański, Z.; Kołacz, R.; Gutarowska, B. Odour reducing microbial-mineral additive for poultry manure treatment. *Front. Environ. Sci. Eng.* **2017**, *11*, 1–9. [CrossRef]
8. Joiner, A. Review of the extrinsic stain removal and enamel/dentine abrasion by a calcium carbonate and perlite containing whitening toothpaste. *Int. Dent. J.* **2006**, *56*, 175–180. [CrossRef]
9. Puga, A.; Rosales, E.; Pazos, M.; Sanromán, M.A. Prompt removal of antibiotic by adsorption/electro-Fenton degradation using an iron-doped perlite as heterogeneous catalyst. *Process Saf. Environ. Prot.* **2020**, *144*, 100–110. [CrossRef]
10. Esmaielpour, M.; Akhlaghinia, B.; Jahanshahi, R. Green and efficient synthesis of aryl/alkylbis(indolyl)methanes using Expanded Perlite-PPA as a heterogeneous solid acid catalyst in aqueous media. *J. Chem. Sci.* **2017**, *129*, 313–328. [CrossRef]

11. Xue, H.; Jiang, Y.; Yuan, K.; Yang, T.; Hou, J.; Cao, C.; Feng, K.; Wang, X. Floating photocatalyst of B-N-TiO_2/expanded perlite: A sol-gel synthesis with optimized mesoporous and high photocatalytic activity. *Sci. Rep.* **2016**, *6*, 2–10. [CrossRef] [PubMed]
12. Hosseini, M.M.; Kolvari, E.; Vahidian, M.; Bagheri, R. Nano perlite sulfuric acid: An inexpensive heterogeneous acid catalyst for the synthesis of 1, 8-dioxo-octahydroxanthenes and tetrahydrobenzoxanthenes under solvent-free conditions. *J. Appl. Chem.* **2017**, *11*, 109–118.
13. Modiba, E.; Osifo, P.; Rutto, H. The use of impregnated perlite as a heterogeneous catalyst for biodiesel production from marula oil. *Chem. Pap.* **2014**, *68*, 1341–1349. [CrossRef]
14. Abrouki, Y.; Anouzla, A.; Loukili, H.; Chakir, A.; Abrouki, K.; Loukili, M.; Rayadh, A.; Bahlaoui, M.A.; Zahouily, M.; Kacemi, K.E.; et al. Investigation of the basis for catalytic activity of expanded Perlite in Knoevnagel condensation. *Adv. Res. J. Chem. Mater. Sci.* **2013**, *1*, 1–7.
15. Shokrollahzadeh, S.; Abassi, M.; Ranjbar, M. A new nano-ZnO/perlite as an efficient catalyst for catalytic ozonation of azo dye. *Environ. Eng. Res.* **2019**, *24*, 513–520. [CrossRef]
16. Radonjić, V.D.; Krstić, J.B.; Lončarević, D.; Vukelić, N.; Jovanović, D.M. Mg-ni supported on perlite as hydrogenation catalyst: Influence of mg and ni content. *Chem. Ind. Chem. Eng. Q.* **2019**, *25*, 193–206. [CrossRef]
17. Malpani, S.K.; Goyal, D.; Katara, S.; Rani, A. Turkish perlite supported nickel oxide as the heterogeneous acid catalyst for a series of Claisen–Schmidt condensation reactions. *Turk. J. Chem.* **2021**, *45*, 1097–1114. [CrossRef] [PubMed]
18. Goyal, D.; Priyanka; Hada, R.; Katara, S.; Bhatia, A.; Kabra Malpani, S. Development of green, effective, and cost-efficient perlite supported solid base catalyst and application in condensation reactions. *Mater. Today Proc.* **2021**, *49*, 3717–3725. [CrossRef]
19. Goyal, D.; Saikia, H.; Hada, R.; Katara, S.; Bhatia, A.; Malpani, S.K. Perlite supported cobalt oxide catalyst for a series of liquidphase esterification reactions. *Macromol. Symp.* **2022**, *402*, 2100369. [CrossRef]
20. Umamaheswari, V.; Palanichamy, M.; Arabindoo, B.; Murugesan, V. Regioselective t-butylation of m-cresol over mesoporous Al-MCM-41 molecular sieves. *Indian J. Chem.—Sect. A Inorg. Phys. Theor. Anal. Chem.* **2000**, *39A*, 1241–1247.
21. Yadav, G.D.; Pathre, G.S. Novel mesoporous solid superacids for selective C-alkylation of m-cresol with tert-butanol. *Microporous Mesoporous Mater.* **2006**, *89*, 16–24. [CrossRef]
22. Muraleedharan, L.; Chandrashekara, M.; Prakash, S.J.; Bhat, S. Clay-Based Solid Acid Catalyst for the Alkylation of p-Cresol with tert-Butyl Alcohol. *ChemistrySelect* **2018**, *3*, 801–808. [CrossRef]
23. Bhatt, N.; Patel, A. Liquid phase tert-butylation of cresols catalysed by 12-tungstophosphoricacid and 12-tungstosilicicacid supported onto neutral alumina. *Catal. Lett.* **2007**, *113*, 99–103. [CrossRef]
24. Chandra, K.G.; Sharma, M.M. Alkylation of phenol with MTBE and other tert-butyl ethers: Cation exchange resins as catalysts. *Catal. Lett.* **1993**, *19*, 309–317. [CrossRef]
25. Su, Z.R.; Wang, T.J. 12-Tungstophosphoric acid immobilized on modified macroporous phenol-furfural sulfonic acid resin for tert-butylation of p-cresol. *React. Funct. Polym.* **1995**, *28*, 97–102. [CrossRef]
26. Devassy, B.M.; Shanbhag, G.V.; Lefebvre, F.; Halligudi, S.B. Alkylation of p-cresol with tert-butanol catalyzed by heteropoly acid supported on zirconia catalyst. *J. Mol. Catal. A Chem.* **2004**, *210*, 125–130. [CrossRef]
27. Campbell, C.B.; Onopchenko, A.; Young, D.C. Amberlyst- 15t-Catalyzed Alkylation of Phenolics with Branched Alkenes. Rearrangement of tert -Alkylphenols and Catechols to sec -Alkyl Isomers. *Ind. Eng. Chem. Res.* **1990**, *29*, 642–647. [CrossRef]
28. Yadav, G.D.; Thorat, T.S. Kinetics of alkylation of p-cresol with isobutylene catalyzed by sulfated zirconia. *Ind. Eng. Chem. Res.* **1996**, *35*, 721–731. [CrossRef]
29. Rahman, N.J.A.; Ramli, A.; Jumbri, K.; Uemura, Y. Tailoring the surface area and the acid–base properties of ZrO_2 for biodiesel production from *Nannochloropsis* sp. *Sci. Rep.* **2019**, *9*, 16223. [CrossRef] [PubMed]
30. Berrones, R.; Camas, K.; Pérez, Y.; Ramírez, E.; Pérez, A.; Eapen, D.; Sebastian, P.J. Synthesis and performance of sulfated zirconia catalyst in esterification of oleic acid. *J. New Mater. Electrochem. Syst.* **2014**, *17*, 99–104. [CrossRef]
31. Kauppi, E.I.; Honkala, K.; Krause, A.O.I.; Kanervo, J.M.; Lefferts, L. ZrO_2 Acting as a Redox Catalyst. *Top. Catal.* **2016**, *59*, 823–832. [CrossRef]
32. Kuwahara, Y.; Kaburagi, W.; Fujitani, T. Catalytic conversion of levulinic acid and its esters to γ-valerolactone over silica-supported zirconia catalysts. *Bull. Chem. Soc. Jpn.* **2014**, *87*, 1252–1254. [CrossRef]
33. Ward, A.J.; Pujari, A.A.; Costanzo, L.; Masters, A.F.; Maschmeyer, T. Ionic liquid-templated preparation of mesoporous silica embedded with nanocrystalline sulfated zirconia. *Nanoscale Res. Lett.* **2011**, *6*, 192. [CrossRef] [PubMed]
34. Abdel Salam, M.S.; Betiha, M.A.; Shaban, S.A.; Elsabagh, A.M.; Abd El-Aal, R.M.; El kady, F.Y. Synthesis and characterization of MCM-41-supported nano zirconia catalysts. *Egypt. J. Pet.* **2015**, *24*, 49–57. [CrossRef]
35. Tamizhdurai, P.; Sakthinathan, S.; Santhana Krishnan, P.; Ramesh, A.; Mangesh, V.L.; Abilarasu, A.; Narayanan, S.; Shanthi, K.; Chiu, T.W. Catalytic activity of ratio-dependent SBA-15 supported zirconia catalysts for highly selective oxidation of benzyl alcohol to benzaldehyde and environmental pollutant heavy metal ions detection. *J. Mol. Struct.* **2019**, *1176*, 650–661. [CrossRef]
36. Dong, S.; Zhu, M.; Dai, B. Synthesis, Characterization and Application of ZS/HMS Catalyst in the Esterification of Gossypol. *Green Sustain. Chem.* **2012**, *2*, 8–13. [CrossRef]
37. Kim, K.D.; Kim, J.; Teoh, W.Y.; Kim, J.C.; Huang, J.; Ryoo, R. Cascade reaction engineering on zirconia-supported mesoporous MFI zeolites with tunable Lewis-Brønsted acid sites: A case of the one-pot conversion of furfural to γ-valerolactone. *RSC Adv.* **2020**, *10*, 35318–35328. [CrossRef]

38. Bikmetova, L.I.; Kazantsev, K.V.; Zatolokina, E.V.; Dzhikiya, O.V.; Smolikov, M.D.; Belyi, A.S. Sulfated zirconia catalysts supported on alumina for hexane isomerization. *AIP Conf. Proc.* **2020**, *2301*, 030002.
39. Khatri, C.; Mishra, M.K.; Rani, A. Synthesis and characterization of fly ash supported sulfated zirconia catalyst for benzylation reactions. *Fuel Process. Technol.* **2010**, *91*, 1288–1295. [CrossRef]
40. Mishra, M.; Devi, K.R.S.; Pinheiro, D.; Nizam, A. Zirconia Supported on Rice Husk Silica from Biowaste: A Novel, Efficient, and Recoverable Nanocatalyst for the Green Synthesis of Tetrahydro-1-benzopyrans. *Russ. J. Org. Chem.* **2020**, *56*, 1784–1789. [CrossRef]
41. Mishra, M.K.; Tyagi, B.; Jasra, R.V. Synthesis and characterization of nano-crystalline sulfated zirconia by sol-gel method. *J. Mol. Catal. A Chem.* **2004**, *223*, 61–65. [CrossRef]
42. Yurdakoç, M.; Akçay, M.; Tonbul, Y.; Yurdakoç, K. Acidity of silica-alumina catalysts by amine titration using Hammett indicators and FT-IR study of pyridine adsorption. *Turk. J. Chem.* **1999**, *23*, 319–327.
43. Akkari, R.; Ghorbel, A.; Essayem, N.; Figueras, F. Synthesis and characterization of mesoporous silica-supported nano-crystalline sulfated zirconia catalysts prepared by a sol-gel process: Effect of the S/Zr molar ratio. *Appl. Catal. A Gen.* **2007**, *328*, 43–51. [CrossRef]
44. Devi, K.R.S.; Jayashree, S. Eco friendly nitration of toluene using modified zirconia. *Bull. Chem. React. Eng. Catal.* **2013**, *7*, 205–214. [CrossRef]
45. Kalapathy, U.; Proctor, A.; Shultz, J. A simple method for production of pure silica from rice hull ash. *Fuel Energy Abstr.* **2001**, *42*, 45. [CrossRef]
46. Jain, D.; Khatri, C.; Rani, A. Synthesis and characterization of novel solid base catalyst from fly ash. *Fuel* **2011**, *90*, 2083–2088. [CrossRef]
47. Liu, E.; Locke, A.J.; Frost, R.L.; Martens, W.N. Sulfated fibrous ZrO_2/Al_2O_3 core and shell nanocomposites: A novel strong acid catalyst with hierarchically macro-mesoporous nanostructure. *J. Mol. Catal. A Chem.* **2012**, *353–354*, 95–105. [CrossRef]
48. Marakatti, V.S.; Shanbhag, G.V.; Halgeri, A.B. Sulfated zirconia; An efficient and reusable acid catalyst for the selective synthesis of 4-phenyl-1,3-dioxane by Prins cyclization of styrene. *Appl. Catal. A Gen.* **2013**, *451*, 71–78. [CrossRef]
49. Delarmelina, M.; Deshmukh, G.; Goguet, A.; Catlow, C.R.A.; Manyar, H. Role of Sulfation of Zirconia Catalysts in Vapor Phase Ketonization of Acetic Acid. *J. Phys. Chem. C* **2021**, *125*, 27578–27595. [CrossRef] [PubMed]
50. Saikia, B.J.; Parthasarathy, G. Fourier Transform Infrared Spectroscopic Characterization of Kaolinite from Assam and Meghalaya, Northeastern India. *J. Mod. Phys.* **2010**, *1*, 206–210. [CrossRef]
51. Sharma, S.D.; Singh, S. Synthesis and Characterization of Highly Effective Nano Sulfated Zirconia over Silica: Core-Shell Catalyst by Ultrasonic Irradiation. *Am. J. Chem.* **2013**, *2013*, 96–104.
52. Yadav, G.D.; Ajgaonkar, N.P.; Varma, A. Preparation of highly superacidic sulfated zirconia via combustion synthesis and its application in Pechmann condensation of resorcinol with ethyl acetoacetate. *J. Catal.* **2012**, *292*, 99–110. [CrossRef]
53. Rodríguez-Castellón, E.; Jiménez-López, A.; Maireles-Torres, P.; Jones, D.J.; Rozière, J.; Trombetta, M.; Busca, G.; Lenarda, M.; Storaro, L. Textural and structural properties and surface acidity characterization of mesoporous silica-zirconia molecular sieves. *J. Solid State Chem.* **2003**, *175*, 159–169. [CrossRef]
54. Sepehrian, H.; Khanchi, A.R.; Rofouei, M.K.; Husain, S.W. Non-thermal synthesis of mesoporous zirconium silicate and its characterization. *J. Iran. Chem. Soc.* **2006**, *3*, 253–257. [CrossRef]
55. Parry, E.P. An Infrared Study of Pyridine Adsorbed on Acidic Solids. Characterization of Surface Acidity. *J. Catal.* **1963**, *2*, 371–379. [CrossRef]
56. Reddy, C.R.; Bhat, Y.S.; Nagendrappa, G.; Prakash, B.S.J. Brønsted and Lewis acidity of modified montmorillonite clay catalysts determined by FT-IR spectroscopy. *Catal. Today* **2009**, *141*, 157–160. [CrossRef]
57. Musthofa, M.; Karim, A.H.; Ahmad Fadzlillaah, N.; Rozali Annuar, N.H.; Abdul Jalil, A.; Triwahyono, S. Determination of Lewis and Brönsted acid sites by gas flow-injection technique. *Malays. J. Fundam. Appl. Sci.* **2014**, *6*, 127–131. [CrossRef]
58. Wang, Z.; Navarrete, J. Keggin Structure and Surface Acidity of 12-Phosphotungstic Acid Grafted Zr-MCM-48 Mesoporous Molecular Sieves. *World J. Nano Sci. Eng.* **2012**, *2*, 134–141. [CrossRef]
59. Malpani, S.K.; Goyal, D.; Katara, S.; Rani, A. Green, efficient and economical coal fly ash based phosphomolybdic acid catalysts: Preparation, characterization and application. *Chem. Pap.* **2021**, *75*, 3017–3034. [CrossRef]
60. Hussain, T.S.; Mazhar, M.; Gul, S. Increase in concentration and strength of acidic catalytic sites on sulfated zirconia by doping with silica. *Cuihua Xuebao/Chin. J. Catal.* **2007**, *28*, 622–626. [CrossRef]
61. Ahmed, M.A. Surface characterization and catalytic activity of sulfated-hafnia promoted zirconia catalysts for n-butane isomerization. *Fuel Process. Technol.* **2011**, *92*, 1121–1128. [CrossRef]
62. Sun, Y.; Yuan, L.; Ma, S.; Han, Y.; Zhao, L.; Wang, W.; Chen, C.L.; Xiao, F.S. Improved catalytic activity and stability of mesostructured sulfated zirconia by Al promoter. *Appl. Catal. A Gen.* **2004**, *268*, 17–24. [CrossRef]
63. Rachmat, A.; Trisunaryanti, W.; Wijaya, K. Synthesis and characterization of sulfated zirconia mesopore and its application on lauric acid esterification. *Mater. Renew. Sustain. Energy* **2017**, *6*, 1–9. [CrossRef]
64. Bautista, P.; Faraldos, M.; Yates, M.; Bahamonde, A. Influence of sulphate doping on Pd/zirconia based catalysts for the selective catalytic reduction of nitrogen oxides with methane. *Appl. Catal. B Environ.* **2007**, *71*, 254–261. [CrossRef]
65. Genov, K.; Georgiev, V.; Batakliev, T.; Sarker, D.K. Ozone decomposition over silver-loaded perlite. *World Acad. Sci. Eng. Technol.* **2011**, *80*, 1015–1018.

66. Negrón-Silva, G.; Hernández-Reyes, C.X.; Angeles-Beltrán, D.; Lomas-Romero, L.; González-Zamora, E.; Méndez-Vivar, J. Comparative study of the regioselective synthesis of β-aminoalcohols under solventless conditions catalyzed by sulfated zirconia and SZ/MCM-41. *Molecules* **2007**, *12*, 2515–2532. [CrossRef] [PubMed]
67. Wang, J.A.; Chen, L.F.; Noreña, L.E.; Navarrete, J.; Llanos, M.E.; Contreras, J.L.; Novaro, O. Mesoporous structure, surface acidity and catalytic properties of Pt/Zr-MCM-41 catalysts promoted with 12-tungstophosphoric acid. *Microporous Mesoporous Mater.* **2008**, *112*, 61–76. [CrossRef]
68. Kondamudi, K.; Elavarasan, P.; Dyson, P.J.; Upadhyayula, S. Alkylation of p-cresol with tert-butyl alcohol using benign Bronsted acidic ionic liquid catalyst. *J. Mol. Catal. A Chem.* **2010**, *321*, 34–41. [CrossRef]
69. Bartholomew, C.H. Mechanisms of catalyst deactivation. *Appl. Catal. A Gen.* **2001**, *212*, 17–60. [CrossRef]
70. Molnár, Á.; Papp, A. Catalyst recycling—A survey of recent progress and current status. *Coord. Chem. Rev.* **2017**, *349*, 1–65. [CrossRef]